Submitted to ApJ, 2014 Mar 26
Preprint typeset using LaTeX style emulateapj v. 5/2/11

arXiv:1403.6751v1 [astro-ph.HE] 26 Mar 2014

A HARD X-RAY POWER-LAW SPECTRAL CUTOFF IN CENTAURUS X-4

Deepto Chakrabarty[1], John A. Tomsick[2], Brian W. Grefenstette[3], Dimitrios Psaltis[4], Matteo Bachetti[5,6], Didier Barret[5,6], Steven E. Boggs[2], Finn E. Christensen[7], William W. Craig[8,2], Felix Fürst[3], Charles J. Hailey[9], Fiona A. Harrison[3], Victoria M. Kaspi[10], Jon M. Miller[11], Michael A. Nowak[1], Vikram Rana[3], Daniel Stern[12], Daniel R. Wik[13], Jörn Wilms[14], William W. Zhang[13]

Submitted to ApJ, 2014 Mar 26

ABSTRACT

The low-mass X-ray binary Cen X-4 is the brightest and closest (<1.2 kpc) quiescent neutron star transient. Previous 0.5–10 keV X-ray observations of Cen X-4 in quiescence identified two spectral components: soft thermal emission from the neutron star atmosphere and a hard power-law tail of unknown origin. We report here on a simultaneous observation of Cen X-4 with *NuSTAR* (3–79 keV) and *XMM-Newton* (0.3–10 keV) in 2013 January, providing the first sensitive hard X-ray spectrum of a quiescent neutron star transient. The 0.3–79 keV luminosity was $1.1 \times 10^{33}\, D^2_{\rm kpc}$ erg s^{-1}, with $\simeq$60% in the thermal component. We clearly detect a cutoff of the hard spectral tail above 10 keV, the first time such a feature has been detected in this source class. Comptonization and synchrotron shock origins for the hard X-ray emission are ruled out on physical grounds. However, the hard X-ray spectrum is well fit by a thermal bremsstrahlung model with kT_e=18 keV, which can be understood as arising in a radiatively-inefficient accretion flow (RIAF) if only a small fraction of the mass flow reaches the neutron star. We suggest that most of the accretion flow is centrifugally inhibited by the magnetic propeller effect. The power-law cutoff energy is set by the degree of Compton cooling of the RIAF electrons by thermal seed photons from the neutron star atmosphere. Lower thermal luminosities should lead to higher (possibly undetectable) cutoff energies. We compare Cen X-4's behavior with PSR J1023+0038, IGR J18245−2452, and XSS J12270−4859, which have shown transitions between LMXB and radio pulsar modes at a similar X-ray luminosity.

Subject headings: accretion, accretion disks — binaries: close — stars: neutron — stars: individual (Cen X-4) — X-rays: binaries

1. INTRODUCTION

Low-mass X-ray binaries (LMXBs) consist of a neutron star (NS) or black hole (BH) accreting from a low-mass ($\lesssim 1\ M_\odot$) stellar companion via Roche-lobe overflow. They may be divided into two categories: persistent accretors with X-ray luminosity $L_{\rm x} \gtrsim 10^{36}$ erg s^{-1}, and transient systems. Transient LMXBs undergo recurrent bright ($L_{\rm x} \gtrsim 10^{36}$ erg s^{-1}) outbursts lasting days to weeks and then return to long intervals of X-ray quiescence ($L_{\rm x} \lesssim 10^{34}$ erg s^{-1}) lasting months to years. The long-term average mass accretion rate of the transients is thus substantially lower than in the persistent systems, owing to their low duty cycle. Transient behavior is understood to arise from a thermal instability in the outer accretion disk wherein the viscosity (and thus $\dot{M}$ through the disk) jumps to a higher value when a critical surface density is reached as the disk fills up (see Lasota 2001, and references therein). The persistent LMXBs are able to avoid this instability because their higher accretion rates lead to increased X-ray heating, keeping the disks permanently ionized (van Paradijs 1996; King, Kolb, & Burderi 1996).

For the NS systems, the 0.5–10 keV X-ray spectrum of quiescent LMXB transients typically consists of two components: a low-energy ("soft") ∼0.1 keV thermal component, and a high-energy ("hard") power-law component with photon index $1 < \Gamma < 2$, where photon flux $dN/dE \propto E^{-\Gamma}$. The soft component is generally well fit by a hydrogen atmosphere model for the NS. The leading explanation for the energy source of the soft component is a deep crustal heating model (Brown, Bildsten & Rutledge 1998) in which the emission is powered by heat injected into the NS crust by pycnonuclear reactions driven by accretion during transient outbursts. In this model, the

[1] MIT Kavli Institute for Astrophysics and Space Research, Massachusetts Institute of Technology, Cambridge, MA 02139, USA. deepto@mit.edu
[2] Space Sciences Laboratory, University of California, Berkeley, CA 94720, USA.
[3] Cahill Center for Astronomy and Astrophysics, California Institute of Technology, Pasadena, CA 91125, USA
[4] Department of Astronomy, University of Arizona, Tucson, AZ 85721, USA
[5] Observatoire Midi-Pyrénées, Université de Toulouse III – Paul Sabatier, 31400 Toulouse, France
[6] CNRS, Institut de Recherche en Astrophysique et Planetologie, 31028 Toulouse, France
[7] Division of Astrophysics, National Space Institute, Technical University of Denmark, 2800 Lyngby, Denmark
[8] Lawrence Livermore National Laboratory, Livermore, CA 94550, USA
[9] Columbia Astrophysics Laboratory, Columbia University, New York, NY 10027, USA
[10] Department of Physics, McGill University, Montreal, PQ, H3A 2T8, Canada
[11] Department of Astronomy, University of Michigan, Ann Arbor, MI 48109, USA
[12] Jet Propulsion Laboratory, California Institute of Technology, Pasadena, CA 91109, USA
[13] Astrophysics Science Division, NASA Goddard Space Flight Center, Greenbelt, MD 20771, USA
[14] Dr. Karl-Remeis-Sternwarte and Erlangen Centre for Astroparticle Physics, Universität Erlangen-Nürnberg, D-96049 Bamberg, Germany

contribution of quiescent accretion is negligible. X-ray spectroscopy of soft thermal emission in quiescent NS transients has been used to infer NS radii (Brown, Bildsten & Rutledge 1998; Rutledge et al. 1999; Guillot et al. 2013) and to study the thermal relaxation of NS crusts (see Wijnands, Degenaar, & Page 2013, and references therein). However, a possible problem for such studies is that accretion may not have completely shut off during quiescence, as suggested by the detection of quiescent variability in the two brightest quiescent NS/LMXBs, Aql X-1 (Rutledge et al. 2002) and Cen X-4 (Campana et al. 2004; Bernardini et al. 2013). There has been considerable debate as to whether this variability is primarily in the soft thermal component, the hard power-law component, or both (e.g., Rutledge et al. 2002; Campana & Stella 2003; Cackett et al. 2005).

The origin of the hard power-law tail is unclear. It is not predicted by the deep crustal heating model (Brown, Bildsten & Rutledge 1998). Two explanations have been discussed: synchrotron shock emission from a radio pulsar wind and Comptonization of the soft thermal photons by a hot corona (Campana et al. 1998a). The synchrotron model is of particular interest given the recent confirmation that NS/LMXBs can turn on as radio pulsars at low accretion rates (Archibald et al. 2009; Papitto et al. 2013). A difficulty in discriminating between different models has been the absence of knowledge about how high the power-law component extends in energy, owing to lack of sufficient observational sensitivity above 10 keV. The recent launch of the *NuSTAR* hard X-ray telescope provides the first opportunity to explore this question.

The ideal target with which to address this is Cen X-4 = X1455−314 (Galactic coordinates $l = 332.2°$, $b = 23.9°$), the brightest quiescent NS/LMXB. It was discovered in 1969 in the 3–12 keV band with the *Vela 5A/5B* satellites during an extremely bright (∼20 Crab at peak) X-ray outburst lasting over two months (Conner, Evans, & Belian 1969; Evans, Belian, & Conner 1970). A second bright (∼4 Crab at peak) X-ray outburst was detected in 1979 (Kaluzienski, Holt, & Swank 1980) along with counterparts in the optical (Canizares, McClintock, & Grindlay 1980) and radio (Hjellming 1979; Hjellming et al. 1988), but the source has been in X-ray quiescence (∼ $10^5\times$ fainter) ever since.

Bright X-ray flashes, now understood as thermonuclear (type I) X-ray bursts, were observed during both the 1969 and 1979 outbursts (Belian, Conner, & Evans 1972; Matsuoka et al. 1980), conclusively establishing the source as a NS and setting an upper limit on the distance of 1.2±0.3 kpc (Chevalier et al. 1989). The presence of thermonuclear bursts indicates that the surface dipole magnetic field is weak, with $B_{\rm surf} \lesssim 10^{10}$ G (Joss & Li 1980) and most likely $\sim 10^8$ G (by analogy with other type I bursters). Optical photometry and spectroscopy indicate that the binary companion V822 Cen is a K3-7 V dwarf, the binary period is 15.1 hr, and the binary mass ratio is $q = 0.1755$ (Chevalier et al. 1989; Torres et al. 2002; D'Avanzo et al. 2005; Shahbaz, Watson, & Dhillon 2014). The best-fit NS mass is $1.94^{+0.37}_{-0.85} M_\odot$ (Shahbaz, Watson, & Dhillon 2014). Given the proximity and high Galactic latitude of the source, it has extremely low interstellar extinction and absorption, allowing more sensitive observations in the ultraviolet and soft X-ray bands than usually possible for LMXBs (Blair et al. 1984; McClintock & Remillard 2000; Park & Garcia 2011; Cackett et al. 2013). The integrated values along this line of sight are $A_V = 0.362$ (Schlafly & Finkbeiner 2011) and $N_{\rm H} \approx 9 \times 10^{20}$ cm^{-2} (Dickey & Lockman 1990; Kalberla et al. 2005).

Cen X-4 has been observed extensively during X-ray quiescence since the 1979 outburst, with deep X-ray spectra in the 0.5–10 keV range previously obtained on six occasions since 1994 (see Cackett et al. 2010, and references therein; see also §5.2). A long-term daily monitoring campaign with *Swift* recently demonstrated that the thermal and power-law components vary together on time scales from days to months, with no spectral change observed and each component contributing roughly half the flux (Bernardini et al. 2013). These authors concluded that the quiescent X-ray emission in Cen X-4 is primarily generated by accretion.

In this paper, we present the first sensitive hard X-ray observation of Cen X-4 in quiescence with *NuSTAR*, obtained simultaneously with a deep *XMM-Newton* soft X-ray observation. We describe the observations in §2 and our spectral analysis and results in §3. We interpret our results in §4 and discuss their implications in §5. A preliminary report on this work was presented by Chakrabarty et al. (2014).

2. OBSERVATIONS

2.1. *NuSTAR*

NuSTAR, the first focusing hard X-ray observatory in orbit, was launched in 2012 and operates in the 3–79 keV range (Harrison et al. 2013). It consists of two co-aligned telescopes, and the two focal planes (FPMA and FPMB) are each covered by a 2×2 array of cadmium-zinc-telluride (CZT) pixel detectors. Our *NuSTAR* observation of Cen X-4 (ObsID 30001004002) began on 2013 January 20, 20:20 UT and had an elapsed duration of 219 ks, with an on-source exposure time of 114 ks. The source was imaged on detector 0 in both FPMA and FPMB. The data were processed and screened using the standard pipeline for on-axis point sources in the *NuSTAR* Data Analysis System (`nustardas`) version 1.2.0, along with the *NuSTAR* calibration database (CALDB) version 20130509. Light curves and spectra from both FPMA and FPMB were extracted from a circular region centered on the source position with a radius of 75 arcsec.

A detailed background model for the source position in each of the two telescopes was derived by using the `nuskybgd` tool (Wik et al. 2014) to fit blank sky regions covering the entire field of view for each focal plane. For faint point sources like Cen X-4, this is more accurate than the usual method of simply scaling from the background of a nearby blank sky region because it correctly accounts for the highly non-uniform background gradients across the detectors. In both telescopes, the background was brighter than the source above around 20 keV. The background-subtracted count rates in FPMA and FPMB were $(4.51 \pm 0.09) \times 10^{-2}$ count s^{-1} and $(4.08 \pm 0.09) \times 10^{-2}$ count s^{-1}, respectively. The *NuSTAR* spectra were rebinned so that all but the highest energy bin had a background-subtracted

significance of at least 10σ. The highest energy bin had 5.2σ significance in FPMA (20–79 keV) and 4.3σ significance in FPMB (17–79 keV), demonstrating that the source was detected beyond 20 keV.

2.2. *XMM-Newton*

The *XMM-Newton* observatory, launched in 1999, is a focusing X-ray telescope operating in the 0.3–12 keV range (Jansen et al. 2001). Our *XMM-Newton* observation of Cen X-4 (ObsID 0692790201) began on 2013 January 21, 13:01 UT and had a duration of 35 ks; this was simultaneous with part of our *NuSTAR* observation. We used the data from all three co-aligned imaging X-ray cameras (EPIC-pn, EPIC-MOS1, and EPIC-MOS2; Strüder et al. 2001; Turner et al. 2001). The cameras were operated in full-frame mode with the thin optical-blocking filter in place, resulting in a time resolution of 73 ms for EPIC-pn and 2.6 s for the MOS cameras. The data were reduced using the *XMM-Newton* Scientific Analysis System (SAS) v13.0.1, along with the latest calibration files available as of 2013 July 13. We reprocessed the data using `epproc` and `emproc` to produce new event files and applied standard event filtering. We identified background flare intervals by constructing a lightcurve of the 10–12 keV EPIC-pn data using events from the entire field of view, and searching for intervals where the count rate exceeded 1 count s^{-1}. We found three short flares; these intervals were removed from our Cen X-4 event lists. The net exposure time was 27 ks for EPIC-pn and 30 ks for each of the EPIC-MOS units.

For all three detectors, we initially extracted light curves and spectra from a circular region centered on the source position with a radius of 43.5 arcsec. For the MOS detectors, we measured the background using a square blank-sky region 3×3 arcmin in size. For the EPIC-pn detector, an important consideration is that the outer parts of the field-of-view include photons due to Cu fluorescence in the instrument while the inner parts do not. As Cen X-4 was in the region without the Cu emission line, we chose a rectangular region near Cen X-4 for determining the EPIC-pn background. The background-subtracted count rates in the 0.3–10 keV range were 2.58 ± 0.01 count s^{-1} in EPIC-pn, 0.640 ± 0.005 count s^{-1} in EPIC-MOS1, and 0.619 ± 0.005 count s^{-1} in EPIC-MOS2.

These count rates are higher than the those observed in previous *XMM-Newton* observations (Cackett et al. 2010). In fact, the count rates in both the EPIC-MOS and EPIC-pn detectors are close to the threshold where photon pileup effects may begin to distort the measured spectra, particularly during the flares[15]. Moreover, our preliminary analysis found that the two EPIC-MOS spectra each have significant systematic differences with the EPIC-pn spectrum above 2 keV. As a precaution, we re-extracted both the MOS and pn data from an annular region centered on the source position with an outer radius of 43.5 arcsec and an inner radius of 10 arcsec, thus excluding the core of the point-spread function (PSF) where any pile-up would occur (at the expense of reduced counting statistics). The MOS and pn spectra from the annular region are mutually consistent. This annulus-only data set still includes sufficient counts to obtain a good measurement of the soft X-ray spectrum.

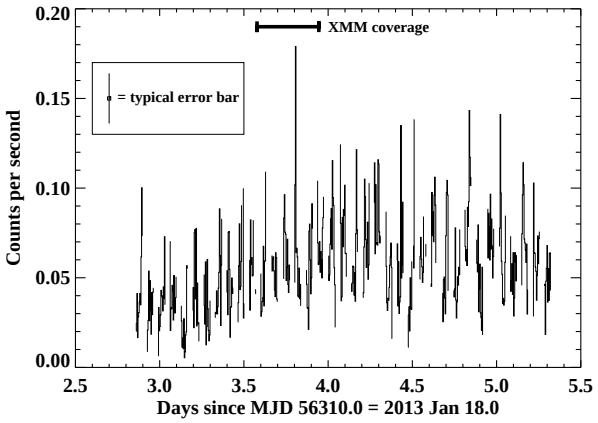

Figure 1. Background-subtracted 3–20 keV light curve of Cen X-4 measured with *NuSTAR*, binned at 300 s resolution. The average of the FPMA and FPMB count rates is plotted, and the size of a typical error bar is shown. The data gaps are due to Earth occulations. The source intensity varies significantly on time scales of minutes to hours. The interval with simultaneous coverage with *XMM-Newton* is indicated, and includes a bright flare around MJD 56313.8 (see Figure 2).

3. DATA ANALYSIS AND RESULTS

3.1. *Timing*

The light curves for the *NuSTAR* and *XMM-Newton* observations are shown in Figure 1 and the top panel of Figure 2, respectively. (The *XMM-Newton* light curve uses the full data set, not the annulus-only data.) Both light curves vary significantly on time scales of a few minutes. The *XMM-Newton* light curve clearly exhibits flaring activity; the strongest of these flares, around MJD 56313.8, is also easily visible in the *NuSTAR* light curve. The fractional excess root-mean-squared (rms) variability[16] $F_{\rm var}$ was 37±6% in the *NuSTAR* light curve and 37±2% in the *XMM-Newton*/EPIC-pn light curve. For comparison, a value of 73.0±1.5% was measured in 60 short *Swift* observations made over three months (Bernardini et al. 2013).

A comparison of the 0.3–1 keV and 2–10 keV *XMM-Newton*/EPIC-pn light curves shows no evidence for significant spectral changes during these flares (Figure 2, bottom panel; Figure 3). We searched the *NuSTAR* light curve for evidence of orbital variability by folding at the 15.1 hr binary period (Shahbaz, Watson, & Dhillon 2014). No orbital modulation was detected.

3.2. *Spectroscopy*

Since there is no evidence for significant spectral variability during the flares (Figure 2, bottom panel; Figure 3), we chose to include the flare intervals for our spectral analysis. We performed joint spectral fits of the *NuSTAR* and *XMM-Newton* (annulus) data with XSPEC

[15] See Table 3 in §3.3.2 of the *XMM-Newton Users Handbook*, v2.11, 2013, `http://heasarc.gsfc.nasa.gov/docs/xmm/uhb/`.

[16] This is a meausre of the intrinsic source variability in excess of Poisson counting noise; see, e.g., Vaughan et al. (2003).

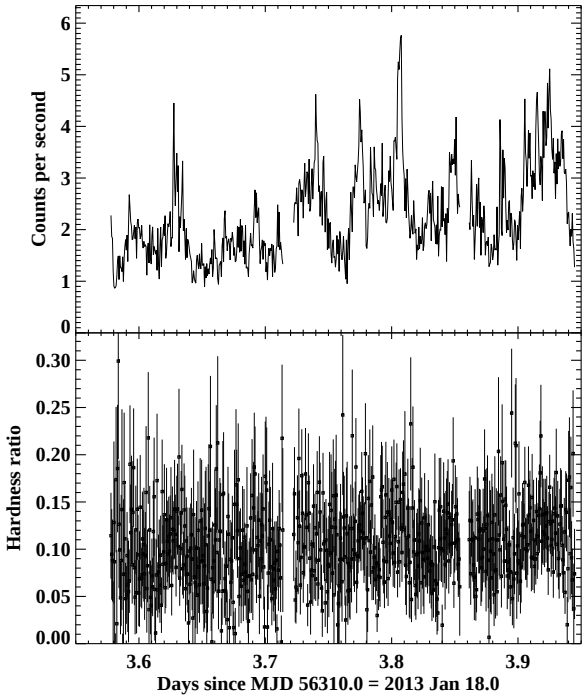

Figure 2. *Top panel:* Background-subtracted 0.3–10 keV light curve of Cen X-4 measured with *XMM-Newton*/EPIC-pn, binned at 50 s resolution. The typical error bar is ± 0.16 counts s^{-1}. The short data gaps are intervals which were excluded owing to strong backgroud flares. The source intensity shows strong flaring behavior, varying by more than a factor of two on time scales as short as a few minutes. The brightest flare, around MJD 56313.8, is also visible in the *NuSTAR* light curve (see Figure 1). *Bottom panel:* Spectral hardness of the count rate shown in the top panel, constructed by taking the ratio of the 2–10 keV and 0.3–1.0 keV count rates. There is no evidence for significant spectral changes during the flaring intervals.

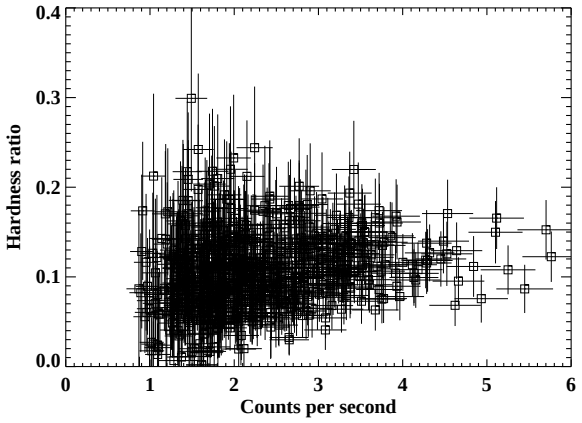

Figure 3. Hardness-intensity diagram for *XMM-Newton*/EPIC-pn observation of Cen X-4. The x-axis shows the 0.3–10 keV count rate, and the y-axis shows the spectral hardness (defined as the ratio of the 2–10 keV and 0.3–1.0 keV count rates). There is no evidence for significant spectral changes as a function of source intensity.

version 12.8 spectral fitting software (Arnaud 1996) using χ^2-minimization. To allow for systematic calibration differences between the different detectors, we included

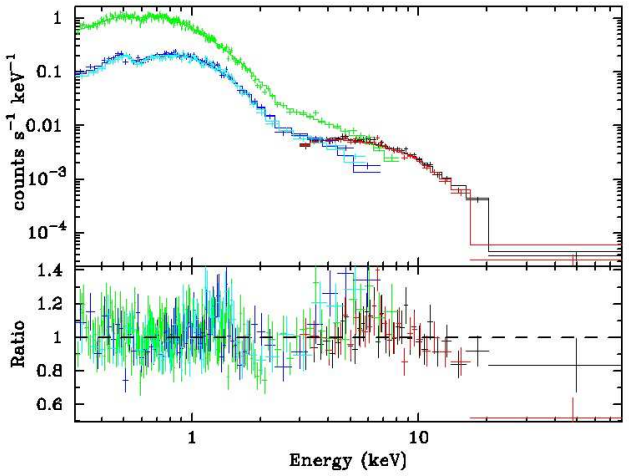

Figure 4. Count spectrum and fit for our joint *XMM-Newton* and *NuSTAR* observation of Cen X-4, using an unbroken power-law to model the hard X-ray spectrum. The model used is `tbabs*(nsatmos+powerlaw)`. The *XMM-Newton* data were extracted from an annulus in order to avoid possible photon pileup effects (see §2.2). The green points are the *XMM-Newton* EPIC-pn data; the dark and light blue points are the *XMM-Newton* EPIC MOS1 and MOS2 data, respectively; and the black and red points are the *NuSTAR* FPMA and FPMB data, respectively. The residuals are consistent with a break in the power law spectrum around 7 keV or a cutoff in the 10–20 keV range.

a constant multiplicative factor in the model. This constant was set to unity for *XMM-Newton*/EPIC-pn but allowed to vary for the other detectors. All other spectral model parameters were tied together across the three instruments. Interstellar absorption was modeled using the `tbabs` model (Wilms, Allen, & McCray 2000) along with photoionization cross-sections from Verner et al. (1996).

We tried two different models for the soft thermal component. We first fit a passively cooling neutron star atmosphere using the `nsatmos` model (Heinke et al. 2006), which assumes a pure H atmosphere and a negligible surface magnetic field ($B \lesssim 10^8$ G), and also includes the effects of surface gravity, heat conduction by electrons, and self-irradiation. In applying `nsatmos`, we fixed the source distance at 1.2 kpc (Chevalier et al. 1989) and assumed that the atmospheric emission was coming from the entire NS surface. We found that it was not possible to constrain the NS mass M and radius R when both were allowed to vary, as a wide range of M-R pairs gave acceptable fits. We therefore fixed the NS mass to $M = 1.9 M_\odot$ (Shahbaz, Watson, & Dhillon 2014). As an alternative model, we also tried fitting to synthetic spectra of Zampieri et al. (1995, 2001) for thermal emission from unmagnetized NSs with a pure H atmosphere in the presence of very low accretion rates. These spectra have been implemented as the XSPEC additive table model `zamp` and are parametrized in terms of the observed accretion luminosity scaled to the Eddington rate (L_∞/L_E), with fixed NS mass $M = 1.4 M_\odot$ and true radius $R = 12.4$ km. In practice, the model shapes from `nsatmos` and `zamp` are essentially identical (see, e.g. Soria et al. 2011), but it is useful to demonstrate that models that explicitly include accretion are consistent with the data.

Although previous 0.5–10 keV X-ray observations of Cen X-4 in quiescence were all well fit by an ab-

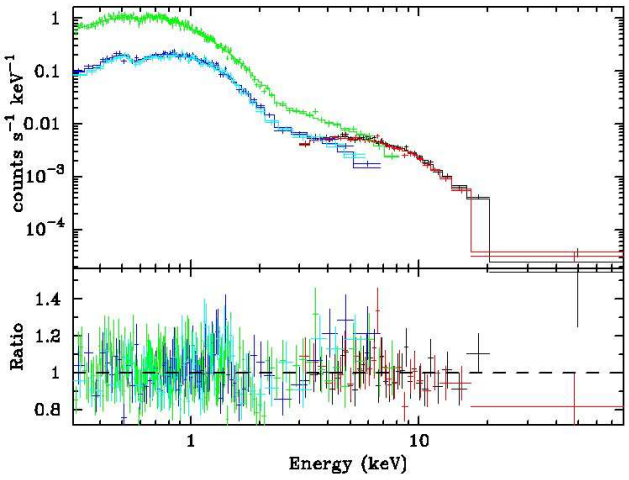

Figure 5. Count spectrum and model fit for our joint *XMM-Newton* and *NuSTAR* observation of Cen X-4, with the hard X-ray spectral cutoff included in the model. A bremsstrahlung model is shown: `tbabs*(nsatmos+bremss)`. The color scheme is the same as in Figure 4. The fit parameters are shown in Table 1.

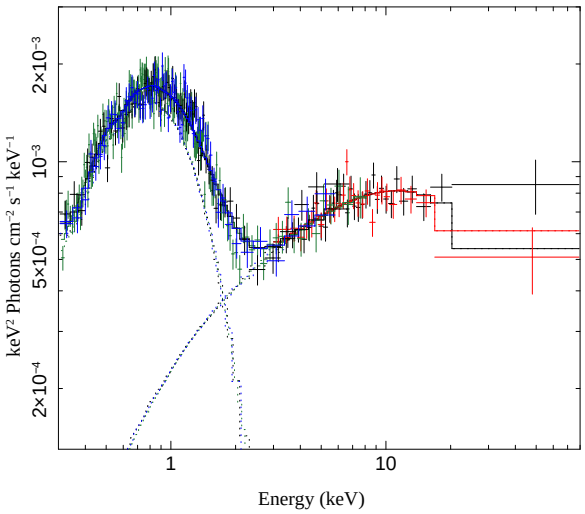

Figure 6. The unfolded νF_ν spectrum of Cen X-4 corresponding to the `tbabs*(nsatmos+bremss)` fit shown in Figure 5. The individual model components are denoted by the dotted lines.

sorbed passive NS atmosphere plus power-law model (see Cackett et al. 2010, and references therein), the `tbabs*(nsatmos+powerlaw)` model does not provide a satisfactory fit to the high-energy data in our combined *NuSTAR*+*XMM-Newton* data covering the 0.3–79 keV range. The residuals indicate the presence of a spectral break in the 10–20 keV range (see Figure 4). We found several different models provided a good fit for the hard component: a cut-off power-law (`cutoffpl`), a broken power-law (`bknpower`), thermal Comptonization (`comptt`; Titarchuk 1994; Hua & Titarchuk 1994), and thermal bremsstrahlung (`bremss`). In each case, this component was combined with `tbabs` and either `nsatmos` or `zamp`. In all cases, the $N_{\rm H}$ value is consistent with the integrated interstellar value along the line of sight (Dickey & Lockman 1990; Kalberla et al. 2005).

The spectral fits with `nsatmos` are summarized in Table 1; those with `zamp` are summarized in Table 2. A typical fit is shown in Figure 5. The corresponding unfolded spectrum is shown in Figure 6. We are able to obtain reasonably good fits with a wide variety of models. We note that the only spectral shape parameter in the `zamp` model is the accretion luminosity L_∞ observed at infinity; one must compare this with the measured flux and source distance to check for self-consistency. We find that the best-fit values of L_∞ are roughly consistent with the measured soft flux for the assumed distance of 1.2 kpc.

Using the `tbabs*(nsatmos+bremss)` model, we find an average (absorbed) flux of 3.8×10^{-12} erg cm^{-2} s^{-1} in the soft (0.3–3 keV) band and 3.3×10^{-12} erg cm^{-2} s^{-1} in the hard (3–79 keV) band. The unabsorbed soft luminosity was $L_{\rm soft}=6.6\times10^{32}D^2_{\rm kpc}$ erg s^{-1} (0.3–3 keV), the unabsorbed hard luminosity was $L_{\rm hard}=4.0\times10^{32}D^2_{\rm kpc}$ erg s^{-1} (3–79 keV), and the total unabsorbed luminosity was $L_x=1.1\times10^{33}D^2_{\rm kpc}$ erg s^{-1} (0.3–79 keV), where $D_{\rm kpc}$ is the source distance in kiloparsecs. For comparison with previous observations, the 0.5–10 keV unabsorbed luminosity was $6.4\times10^{32}D^2_{\rm kpc}$ erg s^{-1}. This is the highest 0.5–10 keV luminosity ever measured from Cen X-4 in quiescence. The next highest observation was 2.6 times fainter in 2001 (Campana et al. 2004), and the faintest observation was 11.5 times fainter in 2009 (Cackett et al. 2010). The thermal (NS atmosphere) contribution to the 0.5–10 keV luminosity on our observation is 59%. This is consistent with previous observations, where the thermal fraction has always been 50–60% (Cackett et al. 2010; Bernardini et al. 2013).

4. INTERPRETING THE SPECTRAL BREAK

We now discuss what can be inferred from our observed high-energy spectral break. We introduce dimensionless variables for parametrizing the NS mass $M=1.9\,M_{1.9}M_\odot$ and radius $R=10\,R_{10}$ km. It is also convenient to scale the luminosity and accretion rate to the Eddington critical values,

$$L_E=2.9\times10^{38}\,M_{1.9}\left(\frac{1+X}{1.7}\right)^{-1}\ {\rm erg\ s^{-1}} \qquad (1)$$

$$\dot M_E=1.8\times10^{-8}\,R_{10}\left(\frac{1+X}{1.7}\right)^{-1}\ M_\odot\ {\rm yr^{-1}}\ , \qquad (2)$$

where $X=0.7$ is the hydrogen mass fraction for cosmic abundances. Our observed luminosities can then be written as $L_{\rm soft}/L_E=2.3\times10^{-6}\,M_{1.9}^{-1}$, $L_{\rm hard}/L_E=1.4\times10^{-6}\,M_{1.9}^{-1}$, and $L_x/L_E=3.8\times10^{-6}\,M_{1.9}^{-1}$. It is clear that the quiescent mass accretion rate $\dot M_{\rm NS}$ onto the NS must also be very low. We can set an upper limit by assigning all of the observed X-ray luminosity to accretion, $\dot M_{\rm NS}\le L_xR/GM$. We then have $\dot M_{\rm NS}/\dot M_E\le 3.7\times10^{-6}\,M_{1.9}^{-1}$. At such extremely low accretion rates, the outer accretion disk is likely to transition into a quasi-spherical, radiatively-ineffcient accretion flow (RIAF) at a transition radius $r_t\sim10^4R_{\rm Sch}\sim6\times10^9\,M_{1.9}$ cm, where $R_{\rm Sch}=2GM/c^2$ is the Schwarzschild radius (Narayan & Yi 1995; Narayan, Mahadevan, & Quataert

Table 1
SPECTRAL FITS WITH A PASSIVE NEUTRON STAR ATMOSPHERE[a]

Parameter	Symbol	Units	Hard spectral component				
			`cutoffpl`	`bknpow`	`comptt(disk)`	`comptt(sphere)`	`bremss`
Absorption and `nsatmos` *parameters*							
Absorption column	$N_{\rm H}$	10^{21} cm^{-2}	0.88(4)	0.89(3)	0.92(4)	0.92(4)	0.87(5)
Temperature	$\log T$	K	6.16(4)	6.18(1)	6.20(27)	6.19(23)	6.20(10)
Mass (fixed)	M	$M_\odot$	1.9	1.9	1.9	1.9	1.9
Radius	R	km	9.2(1.0)	8.6(2.6)	8.5(5.7)	8.6(4.9)	8.1(1.8)
Covering fraction (fixed)	$K_{\rm NS}$	···	1	1	1	1	1
Distance (fixed)	D	kpc	1.2	1.2	1.2	1.2	1.2
Hard spectral component parameters							
Normalization	K	10^{-4}	2.3(2)[b]	2.2(2)[b]	0.7(1)[b]	0.7(1)[b]	4.1(1)[c]
Photon index	Γ	···	1.02(10)	1.26(10)	···	···	···
Cutoff or break energy	E_c, E_b	keV	10.4(1.4)	5.8(3)	···	···	···
Photon index 2	Γ_2	···	···	2.02(5)	···	···	···
Electron temperature	kT_e	keV	···	···	6.4(1.1)	6.4(1.1)	18.2(1.0)
Seed temperature	kT_0	keV	···	···	0.74(8)	0.74(7)	···
Scattering optical depth	$\tau_{\rm es}$	···	···	···	4.0(5)	8.8(1.0)	···
Instrument multiplicative constants							
NuSTAR/FPMA	$C_{\rm FPMA}$	···	1.04(3)	1.03(3)	1.02(3)	1.02(3)	1.09(3)
NuSTAR/FPMB	$C_{\rm FPMB}$	···	1.07(4)	1.05(4)	1.05(4)	1.05(4)	1.12(4)
XMM/EPIC-pn (fixed)	$C_{\rm pn}$	···	1	1	1	1	1
XMM/EPIC-MOS1	$C_{\rm MOS1}$	···	1.04(1)	1.04(1)	1.04(1)	1.03(1)	1.04(1)
XMM/EPIC-MOS2	$C_{\rm MOS2}$	···	0.97(1)	0.97(1)	0.97(1)	0.97(1)	0.97(1)
Fit statistic	χ^2_ν/dof	···	1.155/380	1.123/379	1.130/379	1.129/379	1.167/381

[a] 1σ uncertainties in last digits shown in parentheses.
[b] Flux density at 1 keV in units of photons cm^{-2} s^{-1} keV^{-1}.
[c] $(3.02\times10^{-15}/4\pi D^2)\int n_e^2 dV$ in units of cm^{-5}.

Table 2
SPECTRAL FITS WITH AN ACCRETING NEUTRON-STAR ATMOSPHERE[a]

Parameter	Symbol	Units	Hard spectral component				
			`cutoffpl`	`bknpow`	`comptt(disk)`	`comptt(sphere)`	`bremss`
Absorption and `zamp` *parameters*							
Absorption column	$N_{\rm H}$	10^{21} cm^{-2}	0.89(3)	0.87(6)	0.69(5)	0.69(5)	0.93(5)
Luminosity	$\log L_\infty/L_E$	···	−5.15(3)	−5.13(4)	−4.98(3)	−4.98(3)	−5.19(3)
Mass (fixed)	M	$M_\odot$	1.4	1.4	1.4	1.4	1.4
Radius (fixed)	R	km	12.4	12.4	12.4	12.4	12.4
Normalization	$K_{\rm zamp}$	10^{-3}	1.25(2)[b]	1.25(2)[b]	1.39(2)[b]	1.39(2)[b]	1.23(2)[b]
Hard spectral component parameters							
Normalization	K	10^{-4}	2.5(2)[b]	2.3(2)[b]	0.6(1)[b]	0.6(1)[b]	4.2(1)[c]
Photon index	Γ	···	1.08(9)	1.29(7)	···	···	···
Cutoff or break energy	E_c, E_b	keV	11.2(1.5)	5.9(3)	···	···	···
Photon index 2	Γ_2	···	···	2.03(5)	···	···	···
Electron temperature	kT_e	keV	···	···	7.3(1.6)	7.6(1.7)	17.9(1.0)
Seed temperature	kT_0	keV	···	···	0.81(4)	0.81(4)	···
Scattering optical depth	$\tau_{\rm es}$	···	···	···	3.6(6)	7.8(1.2)	···
Instrument multiplicative constants							
NuSTAR/FPMA	$C_{\rm FPMA}$	···	1.04(3)	1.03(3)	1.01(3)	1.01(3)	1.08(3)
NuSTAR/FPMB	$C_{\rm FPMB}$	···	1.07(3)	1.05(4)	1.04(4)	1.04(4)	1.10(4)
XMM/EPIC-pn (fixed)	$C_{\rm pn}$	···	1	1	1	1	1
XMM/EPIC-MOS1	$C_{\rm MOS1}$	···	1.04(1)	1.04(1)	1.03(1)	1.03(1)	1.03(1)
XMM/EPIC-MOS2	$C_{\rm MOS2}$	···	0.97(1)	0.97(1)	0.97(1)	0.97(1)	0.97(1)
Fit statistic	χ^2_ν/dof	···	1.156/380	1.129/379	1.109/379	1.109/379	1.162/381

[a] 1σ uncertainties in last digits shown in parentheses.
[b] Flux density at 1 keV in units of photons cm^{-2} s^{-1} keV^{-1}.
[c] $(3.02\times10^{-15}/4\pi D^2)\int n_e^2 dV$ in units of cm^{-5}.

1998; Menou et al. 1999).

4.1. *Comptonization*

One way to explain a cutoff power-law spectrum is Comptonization, where soft seed photons (like those from the NS atmosphere) are Compton scattered from a corona of hot electrons. Menou & McClintock (2001) have previously argued that Comptonization of the NS atmosphere photons cannot account for the 1–10 keV power law observed in Cen X-4 because the observed luminosity in the power-law component is too high relative to the soft luminosity. We show here that a Comptonization model for the hard spectral break in Cen X-4 is not physically self-consistent, despite providing an acceptable fit to our observed spectrum. For simplicity, we consider the spherical geometry case; the results for a disk geometry are qualitatively similar.

Our `comptt` fits yielded an electron temperature of $kT_e = 6$–8 keV and an optical depth to electron scattering of $\tau_{\rm es} = 8$–9 for a spherical geometry (see Tables 1 and 2). Theoretically, we expect the optical depth in a corona of radius r_c to be

$$\tau_{\rm es} = \sigma_T \int_R^{r_c} n_e(r) dr \,, \tag{3}$$

where $n_e(r)$ is the electron density and σ_T is the Thomson cross-section. If we assume a RIAF-like spherical accretion flow with a radially uniform mass inflow rate $\dot{M}$ at infall velocity $v_r = \eta\sqrt{GM/r}$, where $\eta \leq 1$, then the electron density must vary with distance r from the NS as

$$n_e(r) = \frac{\dot{M}_{\rm NS}}{4\pi\eta\mu m_p (GMr^3)^{1/2}} \,, \tag{4}$$

where μ is the mean molecular weight and m_p is the proton mass. In this case, we find that the optical depth cannot exceed

$$\tau_{\rm es,max} \approx 10^{-3} \left(\frac{\eta}{0.1}\right)^{-1} \left(\frac{\dot{M}_{\rm NS}/\dot{M}_E}{4\times10^{-6}}\right), \tag{5}$$

which is orders of magnitude smaller than our `comptt` fit values for $\tau_{\rm es}$.

The only way to obtain higher optical depths is to assume that the mass inflow rate $\dot{M}$ varies with r in such a way that only a small amount of mass actually reaches the NS, with the remainder being expelled in some sort of outflow. Following the "ADIOS" (adiabatic inflow-outflow solution) model of Blandford & Begelman (1999), we can parameterize the mass inflow rate in terms of the mass accretion rate onto the NS as

$$\dot{M}(r) = \left(\frac{r}{R}\right)^p \dot{M}_{\rm NS}, \tag{6}$$

where $p > 0$ and R is the NS radius. (The $p = 0$ case corresponds to the radially uniform inflow rate that which we just dismissed.) In this case, the electron density varies as

$$n_e(r) = \frac{2}{\mu\eta\sigma_T R(1+X)} \sqrt{\frac{c^2R}{GM}} \left(\frac{\dot{M}_{\rm NS}}{\dot{M}_E}\right) \left(\frac{r}{R}\right)^{p-3/2} \tag{7}$$

and the optical depth is

$$\tau_{\rm es} = \frac{2}{\mu\eta(1+X)} \sqrt{\frac{c^2R}{GM}} \left(\frac{\dot{M}_{\rm NS}}{\dot{M}_E}\right) \times \int_1^{r_c/R} \left(\frac{r}{R}\right)^{p-3/2} d\left(\frac{r}{R}\right) . \tag{8}$$

The binary separation is $a = 2.8 \times 10^{11}\, M_{1.9}^{1/3}$ cm (Frank, King, & Raine 2002; Shahbaz, Watson, & Dhillon 2014). We require that $r_c < a$, or equivalently that $r_c/R \lesssim 10^5$. Then taking $\dot{M}_{\rm NS}/\dot{M}_E = 4\times10^{-6}$ and $\tau_{\rm es} = 10$, we find $1.4 < p < 1.6$ for $0.1 < \eta < 1$. Even larger p-values are required for smaller coronas. However, such high p-values yield very high electron densities far from the NS, which is problematic for this model because of the significant bremsstrahlung luminosity that would be implied. Taking $p = 1.5$ (uniform density), $r_c/R = 10^5$, and $kT_e = 5$ keV, we predict a bremsstrahlung emission measure $\int n_e^2 dV = 8\times10^{62}$ cm^{-3}, which corresponds to a luminosity of $8.5\times10^{39} D_{\rm kpc}^2$ erg s^{-1} $\approx 40 D_{\rm kpc}^2 L_E$. This is nearly 7 orders of magnitude brighter than the observed quiescent emission! We conclude that a Comptonization model is not physically self-consistent for the hard spectral component in Cen X-4 in quiescence and can be ruled out.

4.2. *Synchrotron shock emission*

Another way of producing a cut-off power-law spectrum is through synchrotron emission. Radio pulsars dissipate their rotational energy via a relativistic wind comprising charged particles and Poynting flux (see Gaensler & Slane 2006, and references therein). Quiescent NS/LMXB transients can turn on as radio pulsars under some circumstances (Stella et al. 1994); this has recently been observed in at least three cases (see §5.3). If Cen X-4 turned on as a radio pulsar during X-ray quiescence, then synchrotron shock emission from the radio pulsar wind interacting with intrabinary material could produce a power-law X-ray spectrum (Campana et al. 1998a). In principle, the synchrotron power-law spectrum should have an exponential cutoff, but this is generally expected to occur at energies in the γ-ray band.

A formalism for the synchrotron shock scenario was developed by Arons & Tavani (1993) for the case of the eclipsing "black widow" millisecond pulsar PSR B1957+20. The relative energetic contribution of Poynting flux and ions in the wind upstream of the shock is described by a magnetization parameter (Kennel & Coroniti 1984),

$$\sigma = \frac{B_1^2}{4\pi\rho_1\gamma_1 c^2}, \tag{9}$$

where B_1, ρ_1, and γ_1 are the magnetic field strength, density, and Lorentz factor of the upstream wind. For a particle-dominated wind (like the one in the Crab Nebula), $\sigma \sim 10^{-3}$, while for a magnetically dominated wind, $\sigma \gg 1$. We consider both these limits. The wind is powered by spin-down of the pulsar with an energy loss rate that we will assume is proportional to the magnetic

dipole radiation,

$$\dot{E} = \frac{4\pi^2 I \dot{P}}{P^3}, \tag{10}$$

where I is the NS moment of inertia and P and $\dot{P}$ are the pulsar spin period and its derivative. Since we don't know P and $\dot{P}$ for Cen X-4, we will scale the surface dipole magnetic field as $B_{\rm surf} = 10^8\, B_8$ G, where we assume

$$B_{\rm surf} = \left(\frac{3c^3 I P \dot{P}}{8\pi^2 R^6}\right)^{1/2}. \tag{11}$$

Thus, for a millisecond pulsar, $\dot{P} = 10^{-20}\, P_{\rm ms}^{-1}\, B_8^2$ and $\dot{E} = 4 \times 10^{35}\, B_8^2\, P_{\rm ms}^{-3}$ erg s^{-1}, where $P_{\rm ms}$ is the NS spin period in millliseconds.

We follow the analysis of Bogdanov et al. (2011) for PSR J1023+0038 and assume that the shock occurs at the inner Lagrangian (L_1) point of the binary, which lies at a distance $r_{L_1} = 1.9 \times 10^{11} M_{1.9}^{1/3}$ cm from the NS (Frank, King, & Raine 2002; Shahbaz, Watson, & Dhillon 2014). The magnetic field strength just upstream from the shock is then (Arons & Tavani 1993)

$$B_1(r_{L_1}) = \left(\frac{\sigma}{1+\sigma}\right)^{1/2} \left(\frac{\dot{E}}{r_{L_1}^2 c f_p}\right)^{1/2} \tag{12}$$

$$= 0.7\, f_p^{-1/2}\, P_{\rm ms}^{-3/2}\, B_8\, \sigma_{-3}^{1/2}\ {\rm G},\ {\rm for}\ \sigma \ll 1 \tag{13}$$

$$= 21\, f_p^{-1/2}\, P_{\rm ms}^{-3/2}\, B_8\ {\rm G},\ {\rm for}\ \sigma \gg 1, \tag{14}$$

where $f_p = \Delta\Omega_p/4\pi$ is the fractional solid angle into which the wind is emitted. The magnetic field downstream of the shock is $B_2 = 3B_1$. Assuming that the shock gives rise to a power-law distribution of electrons with Lorentz factors in the range $\gamma_1 < \gamma < \gamma_m$, we expect a power-law synchrotron spectrum with photon number index $\Gamma \approx 1.5$ over the energy range $E_1 < E < E_c$, with an exponential cutoff at E_c. The lower energy bound is at

$$E_1 = 0.3\, \gamma_1^2\, \hbar\, \omega_{\rm cyc}(B_2) \tag{15}$$

$$= 0.07\, f_p^{-1/2}\, P_{\rm ms}^{-3/2}\, B_8 \left(\frac{\gamma_1}{10^5}\right)^2 \times \left(\frac{\sigma}{10^{-3}}\right)^{1/2}\ {\rm keV},\ {\rm for}\ \sigma \ll 1 \tag{16}$$

$$= 2\, f_p^{-1/2}\, P_{\rm ms}^{-3/2}\, B_8 \left(\frac{\gamma_1}{10^5}\right)^2\ {\rm keV},\ {\rm for}\ \sigma \gg 1\,, \tag{17}$$

and the cutoff energy is

$$E_c = \gamma_m^2\, \hbar\, \omega_{\rm cyc}(B_2) \tag{18}$$

$$= 240\, f_p^{-1/2}\, P_{\rm ms}^{-3/2}\, B_8 \left(\frac{\gamma_m}{10^8}\right)^2 \times \left(\frac{\sigma}{10^{-3}}\right)^{1/2}\ {\rm MeV},\ {\rm for}\ \sigma \ll 1 \tag{19}$$

$$= 7\, f_p^{-1/2}\, P_{\rm ms}^{-3/2}\, B_8 \left(\frac{\gamma_m}{10^6}\right)^2\ {\rm GeV},\ {\rm for}\ \sigma \gg 1\,, \tag{20}$$

where $\omega_{\rm cyc} = eB/m_e c$ is the electron cyclotron frequency, $\sigma_{-3} = \sigma/10^{-3}$, and e and m_e are the charge and mass of the electron. Production of synchrotron photons in the X-ray band requires $\gamma_1 \gtrsim 10^5$. Arons & Tavani (1993) show that $\gamma_m/\gamma_1 \sim m_p/m_e \sim 10^3$, so we expect E_c to be in the MeV to GeV range.

By contrast, our `cutoffpl` fits yielded a very low cutoff energy of $E_c = 10$ keV (see Tables 1 and 2). This requires $\gamma_m \sim 10^5$, which is inconsistent with our expectations from theory. Also, the synchrotron X-ray emission observed from pulsar wind nebulae around young radio pulsars has an unbroken power-law spectrum out to at least 100 keV (see Gaensler & Slane 2006, and references therein). Millisecond radio pulsars have qualitatively similar properties and so are expected to behave in the same way (Stappers et al. 2003). Finally, the only quiescent NS/LMXB in which synchrotron shock emission is definitely thought to have been observed has an unbroken power-law spectrum out to at least 80 keV (PSR J1023+0038; Tendulkar et al. 2014). Taken together, we conclude that a synchrotron shock model is inconsistent with the low cutoff energy we observe in Cen X-4 and can be ruled out.

4.3. *Bremsstrahlung*

A third way of modeling our cut-off spectrum is through thermal bremsstrahlung emission from an optically thin cloud of hot electrons. Our bremsstrahlung fits (see Tables 1 and 2) yielded an electron temperature kT_e =18 keV and an emission measure

$$\int n_e^2\, dV = 1.6 \times 10^{55}\, D_{\rm kpc}^2\ {\rm cm}^{-3}\,. \tag{21}$$

We again assume that $\dot{M}$ varies with distance from the NS according to equation (6) and use equation (7) for n_e. Then, taking $\mu = 0.6$ and $X = 0.7$ for ionized gas with cosmic abundances, the expected emission measure for a cloud of radius r_c is

$$\int n_e^2\, dV = \frac{8\pi R}{p\eta^2\sigma_T^2} \left(\frac{c^2 R}{GM}\right) \left(\frac{\dot{M}_{\rm NS}}{\dot{M}_E}\right)^2 \left(\frac{r_c}{R}\right)^{2p}. \tag{22}$$

Equating this to equation (21), we find that

$$\frac{r_c}{R} \approx 10^{4/p}\, p^{1/2p}\, D_{\rm kpc}^{1/p} \left(\frac{\eta}{0.1}\right)^{1/p} \times \left(\frac{\dot{M}_{\rm NS}/\dot{M}_E}{4\times 10^{-6}}\right)^{-1/p}, \tag{23}$$

which sets the scale for the bremsstrahlung emission region in units of the NS radius R. Requiring $r_c < a$ or equivalently $r_c/R \lesssim 10^5$, we find that $p \gtrsim 0.8$. Alternatively, if we require that the cloud lies inside the RIAF transition radius ($r_c < r_t$ or $r_c/R \lesssim 10^4$), then we find that $p \gtrsim 1$. In either case, only a small fraction $(r_c/R)^{-p} \lesssim 10^{-4}$ of the mass transferred reaches the NS in quiescence; the rest accumulates at large r or is expelled. In particular, we note that most of the bremsstrahlung emission is coming from electrons at large r. For $p = 1$, the electron density $n_{\rm e}$ ranges from 10^{14} cm^{-3} near the NS to 10^{12} cm^{-3} near r_c.

For self-consistency, we should check that the hot electrons in the emission region will survive against inverse Compton cooling by the soft thermal photons from the

NS atmosphere. The Compton radiative power density is (e.g., Rybicki & Lightman 1979)

$$P_C = \left(\frac{4kT_e}{m_e c^2}\right) c\sigma_T n_e U_{\rm ph}, \quad (24)$$

where $U_{\rm ph} = L_{\rm soft}/4\pi r^2 c$ is the photon energy density of the soft photons. The Compton cooling time is then $t_C = (3/2)n_e kT_e/P_C$, or

$$t_C = 1\times10^{-2}\, M_{1.9}^{-1}\left(\frac{r}{R}\right)^2\left(\frac{L_{\rm soft}/L_E}{2\times10^{-6}}\right)^{-1}\ {\rm s}, \quad (25)$$

which is much longer than the infall time $t_r = r/v_r$, or

$$t_r = 6\times10^{-4}\, M_{1.9}^{-1/2}\left(\frac{r}{R}\right)^{3/2}\left(\frac{\eta}{0.1}\right)^{-1}\ {\rm s}. \quad (26)$$

Note that both t_C and t_r are much larger at large r, although we always have $t_C \gg t_r$ for the given scale value of $L_{\rm soft}$. Thus, we see that the bremsstrahlung is physically consistent for our present Cen X-4 observation. A substantially larger $L_{\rm soft}$ would be required for the electrons to be rapidly cooled, in which case the bremsstrahlung emission would be suppressed. Conversely, we would expect a higher bremsstrahlung temperature if the soft thermal luminosity of Cen X-4 were to become significantly lower.

5. DISCUSSION

5.1. *The spectral break in Cen X-4*

We have measured a break in the hard X-ray power-law spectrum of Cen X-4 which can be fit with an exponential cutoff at around 10 keV or a bremsstrahlung spectrum with $kT_e = 18$ keV. This is the first detection of a power-law break in this source class, and it finally permits a more detailed investigation of the origin of the hard component in quiescent NS/LMXBs. For this observation of Cen X-4, we are able to rule out both Comptonization and synchrotron shock emission as the origin of the spectral break. Instead, the hard X-ray spectrum can be self-consistently understood as bremsstrahlung emission, if we assume that most of the accretion flow from the mass donor is prevented from reaching the NS.

The requirement that most of the accretion flow not reach the NS is consistent with the fact that the inferred $\dot{M}_{\rm NS}$ is substantially smaller than the binary mass transfer rate $\dot{M}_T \sim 0.01\dot{M}_{\rm Edd}$ expected for a Roche-lobe–filing main sequence donor in a 15.1 hr binary (e.g., King, Kolb, & Burderi 1996). Moreover, it has previously been noted that RIAF models for quiescent NS transients also require that most of the accretion flow is somehow prevented from reaching the NS (Asai et al. 1998; Menou et al. 1999). A likely scenario is that most of the flow is centrifugally inhibited by the magnetic "propeller effect" (Illarionov & Sunyaev 1975; Ustyugova et al. 2006). This occurs when the magnetosphere extends beyond the corotation radius

$$r_{\rm co} = \left(\frac{GMP^2}{4\pi^2}\right)^{1/3} = 19\, P_{\rm ms}^{2/3}\, M_{1.9}^{1/3}\ {\rm km}, \quad (27)$$

where the Keplerian and stellar angular velocities are equal. We define the magnetospheric radius r_m as the location where the magnetic and material stresses are equal,

$$r_m = \xi\left(\frac{\mu_m^4}{GM\dot{M}^2}\right)^{1/7} = 31\,\xi\, B_8^{4/7}\, M_{1.9}^{-1/7}\, R_{10}^{10/7} \times\left(\frac{\dot{M}/\dot{M}_E}{0.01}\right)^{-2/7}\ {\rm km}, \quad (28)$$

where μ_m is the magnetic dipole moment of the NS, ξ is an order unity constant that depends upon the details of the accretion flow near the magnetosphere (see, e.g., Psaltis & Chakrabarty 1999), and the usual $R^{12/7}$ scaling is modified by the R-dependence of $\dot{M}_E$. In the propeller regime, $r_m > r_{\rm co}$. For ordinary thin-disk magnetic accretion, the accretion is entirely shut off in this regime. Whether material is expelled in a strong or weak outflow, or else accumulates outside $r_{\rm co}$, depends upon details of the disk-magnetophere interaction (Spruit & Taam 1993; D'Angelo & Spruit 2010, 2012; Lii et al. 2013). However for a RIAF flow onto a millisecond pulsar, r_m will generally lie inside the transition radius r_t, so that the flow onto the magnetosphere will be quasi-spherical. In this geometry, a small fraction of the flow is able to reach the NS despite the centrifugal barrier present in the propeller regime (Menou et al. 1999).

The 18 keV electron temperature for the `bremss` model is much lower than the $\gtrsim$100 keV electron temperature expected in a RIAF flow around a black hole (Mahadevan & Quataert 1997). This may be due to Compton cooling by the soft X-ray photons from the NS atmosphere, in which case we would expect T_e to depend upon the luminosity of the soft X-ray emission from the NS atmosphere. Using equation 24, we find the resulting inverse Compton emission would be no more than a few percent of the overall source luminosity, and thus essentially undetectable in our spectrum. Alternatively, if a shock is present at the centrifugal barrier, then the 18 keV electron temperature may reflect the shock temperature of the flow at the magnetospheric boundary, in which case T_e should show dependence upon B, $\dot{M}$, and possibly P. In either case, it seems that the relatively low power-law cutoff energy that we observe must arise from the NS nature of Cen X-4.

5.2. *Variable Cutoff Energy?*

Given that the slope of the hard X-ray power-law spectrum in Cen X-4 has been observed to vary from epoch to epoch (Cackett et al. 2010), it is unlikely that the 18 keV bremsstrahlung spectrum we have measured is a constant feature of the source in quiescence. In fact, we can demonstrate that the hard X-ray cutoff energy in Cen X-4 is likely variable by noting that the departure of the hard X-ray spectrum from an unbroken power-law above ∼6 keV is evident in our 2013 *XMM-Newton* spectrum alone, even without including the *NuSTAR* data. The shape of an 18 keV bremsstrahlung spectrum will show noticeable curvature below 10 keV. On the other hand, all previous deep observations of Cen X-4 in the 0.5–10 keV band are consistent with an unbroken hard X-ray power-law spectrum, indicating a higher cutoff en-

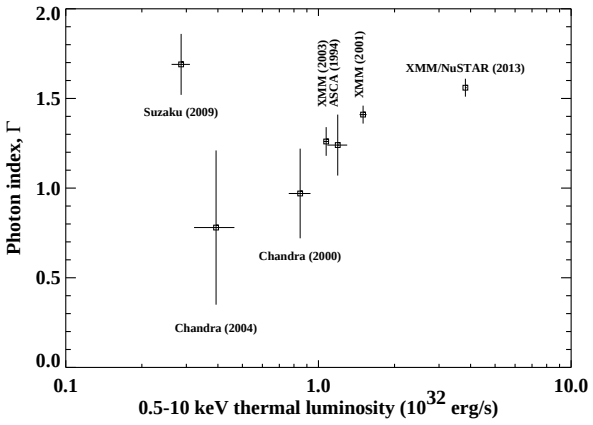

Figure 7. Hard X-ray power-law photon index (2–10 keV) versus unabsorbed 0.5–10 keV thermal luminosity for deep observations of Cen X-4 since 1994. The *XMM/NuSTAR* (2013) point is from a `tbabs*(nsatmos+powerlaw)` fit to the 0.3–10 keV data only, and the archival data are taken from Cackett et al. (2010). The thermal luminosity is computed assuming a distance of 1 kpc. The general trend of steeper power-law slope for higher thermal luminosity is consistent with expectations for bremsstrahlung emission, if we assume that kT_e is reduced from $\gtrsim$100 keV via Compton cooling by thermal photons. At energies well below kT_e, a bremsstrahlung spectrum is a $\Gamma = 1$ power law. The large Γ measured at the lowest thermal luminosity may indicate a transition to synchrotron shock emission at extremely low $\dot{M}$.

ergy for those observations. All of these observations occurred at significantly lower luminosity (see Figure 7). We would expect a lower thermal luminosity to result in reduced Compton cooling of the bremsstrahlung electrons and hence a higher electron temperature, consistent with a higher cutoff energy.

Moreover, we would expect the 2–10 keV power-law slope to vary systematically with the thermal luminosity. For energies far below kT_e, a bremsstrahlung spectrum is a $\Gamma = 1$ power-law (see, e.g. Rybicki & Lightman 1979); as one approaches the cutoff at kT_e from below, the effective Γ over a fixed energy range gradually increases as the spectrum begins to gradually roll over. Thus, if we assume that $kT_e \gtrsim 100$ keV in the absence of Compton cooling, then a bremsstrahlung model predicts that Γ should be close to 1 at low thermal luminosity and should increase as the thermal luminosity rises and kT_e falls. This relationship will eventually break down when kT_e gets sufficiently low, because an unbroken power-law no longer provides even a rough fit to a sharp spectral cutoff. The archival data largely support this picture. In Figure 7, we plot Γ versus thermal luminosity for all the deep observations of Cen X-4 in quiescence made since 1994, including our observation. The archival data are collected from Cackett et al. (2010). The trend of the six brightest observations is consistent with our expectation for a bremsstrahlung model. The one outlier is the lowest luminosity point, for which Γ jumps to 1.7. We suggest below that this may indicate a transition to synchrotron shock emission at the lowest luminosities.

5.3. *Comparison to Other Systems*

It is interesting to compare the behavior of Cen X-4 with systems that have been observed to transition between LMXB and radio pulsar states during X-ray quiescence. The theoretical expectation is that such transitions are controlled by location of the NS magnetospheric boundary (Stella et al. 1994). We can compare r_m to both $r_{\rm co}$ and the light-cylinder radius,

$$r_{\rm lc} = \frac{cP}{2\pi} = 48\, P_{\rm ms}\ {\rm km}\,. \qquad (29)$$

For sufficiently low $\dot{M}$, we have $r_{\rm co} < r_m < r_{\rm lc}$ and the system will be in the propeller regime, with accretion onto the NS (mostly) shut off (Illarionov & Sunyaev 1975; Ustyugova et al. 2006). For even lower $\dot{M}$, we will have $r_{\rm co} < r_{\rm lc} < r_m$. In this case, the radio pulsar mechanism can turn on, with the radiation pressure of a radio pulsar wind clearing the magnetosphere and an intrabinary shock giving rise to synchrotron X-ray emission (Stella et al. 1994; Campana et al. 1998a; Burderi et al. 2001). The $\dot{M}$ implied for transition to a millisecond radio pulsar state corresponds to $L_x \lesssim 10^{33}$ erg s, where the exact value depends on details of the system and the disk-magnetosphere interaction.

Indirect evidence for such transitions in NS/LMXBs during X-ray quiescence was previously reported in Aql X-1 ($L_x = 6 \times 10^{32}$ erg s^{-1}; Campana et al. 1998b) and SAX J1808.4−3658 ($L_x = 5 \times 10^{31}$ Campana et al. 2002; Burderi et al. 2003; Campana et al. 2004). However, more direct evidence has been reported more recently in at least three systems. The 1.7 ms radio pulsar PSR J1023+0038 (hereafter J1023) has made two transitions between the LMXB and radio pulsar states. It is now understood to have been in an LMXB state during 2000–2001, with direct optical evidence for the presence of an accretion disk (Wang et al. 2009). However, a state transition then occurred, with subsequent observations establishing the absence of an accretion disk during 2002–2013 (Thorstensen & Armstrong 2005) as well as the presence of a millisecond eclipsing radio pulsar during 2007–2013 (Archibald et al. 2009), along with a low X-ray luminosity associated with intrabinary synchrotron shock emission (Archibald et al. 2010; Bogdanov et al. 2011). A second state transition was observed more recently, with the radio pulsar turning off and an accretion disk reemerging (Stappers et al. 2013; Patruno et al. 2014).

In all of these observations, J1023 has remained in X-ray quiescence in the sense that a high-luminosity ($L_x \gtrsim 10^{36}$ erg s^{-1}) transient X-ray outburst was not observed. However, two distinct sub-states are evident: a faint X-ray–quiescent state ($L_x \sim 10^{32}$ erg s^{-1}) during which radio pulsations are seen, and a bright X-ray–quiescent state ($L_x \sim 10^{33}$ erg s^{-1}) during which the radio pulsar is off. This suggests that r_m has moved outside the light cylinder in the fainter state. In both sub-states, the 0.3–10 keV X-ray emission has a power-law spectrum with little or no thermal component, with $\Gamma = 1.3$ in the faint state (Archibald et al. 2010) and $\Gamma = 1.69$ in the bright state the bright state (Patruno et al. 2014). *NuSTAR* observations show that these power-law spectra remain unbroken up to at least 79 keV (Tendulkar et al. 2014). During faint X-ray–quiescence, the X-ray flux shows high-amplitude modulation at the orbital period (Archibald et al. 2010; Tendulkar et al. 2014), similar to what is seen in the X-ray emission from some (but not all) eclipsing millisecond radio pulsars (the so-called

"black widow" and "redback" systems; Roberts 2012; Roberts et al. 2014). During bright X-ray–quiescence, the X-ray flux shows strong, rapid flickering, with the intensity varying by an order of magnitude on time scales <100 s (Patruno et al. 2014; Tendulkar et al. 2014).

A second object in which two state LMXB/radio pulsar transitions were seen is the M28 globular cluster source PSR J1824−2452I (hereafter M28I), a 3.9 ms radio pulsar. The radio pulsar underwent a bright transient X-ray outburst ($L_x \sim 10^{36}$ erg s^{-1}) in 2013 March during which accretion-powered millisecond pulsations and a thermonuclear X-ray burst were observed, establishing the system as an NS/LMXB. The system returned to X-ray quiescence within a month, at which point radio pulsations were again detected (Papitto et al. 2013). These observations demonstrate that LMXB/radio pulsar state transitions can occur on time scales as short as days. During X-ray quiescence, rapid ($\lesssim$500 s) intensity variations of nearly an order of magnitude are again seen [$(0.6–4)\times10^{33}$ erg s^{-1}], with no change in the 0.3–10 keV X-ray spectrum: an absorbed power-law with $\Gamma = 1.2$ and no detectable thermal component (Linares et al. 2014). Remarkably, this rapid variability seems to toggle between two stable flux levels; Linares et al. (2014) suggest that this represents fast transitions between synchrotron shock emission and magnetospheric accretion. No orbital variability of the X-ray flux is reported in M28I.

The third object in which an LMXB/radio pulsar transition was seen is XSS J12270−4859 (hereafter J12270), a faint hard X-ray source associated with a relatively bright *Fermi* γ-ray source. During 2003–2012, the source was in a quiescent LMXB state with an absorbed power-law X-ray spectrum with $\Gamma = 1.7$, no evidence for a thermal spectral component, a 0.1–10 keV luminosity of $L_x = 2 \times 10^{33}\, D_{\rm kpc}$ erg s^{-1}, highly variable X-ray flaring, and multiwavelength evidence for the presence of an accretion disk (de Martino et al. 2010, 2013). In late 2012, the source made a transition to a lower ($6 \times 10^{31}\, D_{\rm kpc}$ erg s^{-1}) luminosity state with a power-law X-ray spectrum with $\Gamma = 1.2$, a thermal fraction <9%, and a large-amplitude orbital modulaton of the X-ray flux (Bassa et al. 2014; Bogdanov et al. 2014). After this transition, 1.69 ms radio pulsations were also detected (Roy, Bhattacharyya, & Ray 2014).

Cen X-4 has comparable luminosity to J1023, M28I, and J12270, and so it is presumably at least close to the regime where LMXB/radio transitions could occur. The rapid X-ray variability we observe (see §3.1) is quite different from the large-amplitude orbital modulation seen in the low-quiescent state of J1023, but it is qualitatively similar to the flickering seen in the high-quiescent states of J1023 and J12270 as well as the M28I quiescent variability. On the other hand, unlike those three sources, the X-ray spectrum of Cen X-4 has a substantial thermal fraction ($\simeq$60%). This may indicate that more of the accretion flow reaches the surface of Cen X-4 than in the other systems. If we apply our Cen X-4 bremsstrahlung model to the origin of the hard X-ray emission in J1023, M28I, and J12270, then we would expect a high ($\gtrsim$100 keV) electron temperature in the RIAF corona surrounding these systems and an unbroken power-law X-ray spectrum, consistent with what was observed. Of course, synchrotron shock emission can also produce an unbroken power-law in the X-ray band, and we expect this mechanism to dominate in the radio pulsar state. At sufficiently low luminosity, Cen X-4 should transition into a radio pulsar state; we suggest that this may be what occurred in the lowest luminosity observation shown in Figure 7, and that the sudden jump in Γ might reflect a sharp transition from high-temperature bremsstrahlung emission to synchrotron shock emission. It would be interesting to search for millisecond radio pulsations from Cen X-4 when its X-ray luminosity next drops to $\lesssim 10^{32}\, D_{\rm kpc}$ erg s^{-1}.

D.C. thanks Herman Marshall, Sera Markoff, Carolyn D'Angelo, and Stephen Reynolds for useful discussions, and Luca Zampieri and Roberto Soria for sharing their XSPEC additive table model `zamp`. We also thank Thorsten Brand for help with evaluating the level of photon pileup in the *XMM-Newton* data. This work was supported in part under NASA contract NNG08FD60C and made use of data from the *NuSTAR* mission, a project led by the California Institute of Technology, managed by the Jet Propulsion Laboratory, and funded by NASA. We thank the *NuSTAR* Operations, Software and Calibration teams for support with the execution and analysis of these observations. This research has made use of the *NuSTAR* Data Analysis Software (NuSTARDAS), jointly developed by the ASI Science Data Center (ASDC, Italy) and the California Institute of Technology (USA). JAT acknowledges partial support from the *XMM-Newton* Guest Observer program through NASA grant NNX13AB47G.

Facilities: NuSTAR, XMM.

REFERENCES

Archibald, A. M., Kaspi, V. M., Bogdanov, S., et al. 2010, ApJ, 722, 88
Archibald, A. M., Stairs, I. H., Ransom, S. M., et al. 2009, Science, 324, 1411
Arnaud, K. A. 1996, in ASP Conf. Ser. 101, Astronomical Data Analysis Software and Systems V, ed. G. H. Jacoby & J. Barnes (San Francisco, ASP), 17
Arons, J., & Tavani, M. 1993, ApJ, 403, 249
Asai, K., Dotani, T., Hoshi, R, et al. 1998, PASJ, 50, 611
Bassa, C. G., Patruno, A., Hessels, J. W. T., et al. 2014, MNRAS, submitted (arXiv:1402.0765)
Belian, R. D., Conner, J. P., & Evans, W. D. 1972, ApJ, 171, L87
Bernardini, F., Cackett, E. M., Brown, E. F., et al. 2013, MNRAS, 436, 2465
Blair, W. P., Raymond, J. C., Dupree, A. K., et al. 1984, ApJ, 278, 270
Blandford, R. D., & Begelman, M. C. 1999, MNRAS, 303, L1
Bogdanov, S., Archibald, A. M., Hessels, J. W. T., et al. 2011, ApJ, 742, 97
Bogdanov, S., Patruno, A., Archibald, A. M., et al. 2014, ApJ, submitted (arXiv:1402.6324)
Brown, E. F., Bildsten, L., & Rutledge, R. E. 1998, ApJ, 504, L95
Burderi, L., Di Salvo, T., D'Antona, F., et al. 2003, A&A, 404, L43
Burderi, L., Possenti, A., D'Antona, F., et al. 2001, ApJ, 560, L71
Cackett, E. M., Brown, E. F., Degenaar, N., et al. 2013, MNRAS, 433, 1362
Cackett, E. M., Brown, E. F., Miller, J. M., & Wijnands, R. 2010, ApJ, 720, 1325
Cackett, E. M., Wijnands, R., Heinke, C. O. et al. 2005, ApJ, 620, 922
Campana, S., & Stella, L. 2000, ApJ, 541, 849
Campana, S., & Stella, L. 2003, ApJ, 597, 474

Campana, S., Colpi, M., Mereghetti, S., Stella, L., & Tavani, M. 1998a, A&A Rev., 8, 279
Campana, S., D'Avanzo, P., Cassares, J., et al. 2004, ApJ, 614, L49
Campana, S., Israel, G. L., Stella, L., Gastadello, F., & Mereghetti, S. 2004, ApJ, 601, 474
Campana, S., Stella, L., Gastaldello, F., et al. 2002, ApJ, 575, L15
Campana, S., Stella, L., Mereghetti, S., et al. 1998b, ApJ, 499, L65
Canizares, C. R., McClintock, J. E., & Grindlay, J. E. 1980, ApJ, 236, L55
Chakrabarty, D., Tomsick, J., Grefenstette, B., et al. 2014, AAS Meeting Abstracts, 223, #438.19
Chevalier, C., Ilovaisky, S. A., van Paradijs, J., Pedersen, H., & van der Klis, M. 1989, A&A, 210, 114
Conner, J. P., Evans, W. D., & Belian, R. D. 1969, ApJ, 157, L157
D'Angelo, C. R. & Spruit, H. C. 2010, MNRAS, 406, 1208
D'Angelo, C. R. & Spruit, H. C. 2012, MNRAS, 420, 416
D'Avanzo, P., Campana, S., Casares, J., et al. 2005, A&A, 444, 905
de Martino, D., Belloni, T., Falanga, M., et al. 2013, A&A, 550, A89
de Martino, D., Falanga, M., Bonnet-Bidaud, J.-M., et al. 2010, A&A, 515, A25
Dickey, J. M., & Lockman, F. J. 1990, ARA&A, 28, 215
Evans, W. D., Belian, R. D., & Conner, J. P. 1970, ApJ, 159, L57
Frank, J., King, A., & Raine, D. 2002, Accretion Power in Astrophysics, 3rd ed. (Cambridge U. Press)
Gaensler, B. M., & Slane, P. O. 2006, ARA&A, 44, 17
Guillot, S., Servillat, M., Webb, N. A., & Rutledge, R. E. 2013, ApJ, 772, 7
Harrison, F. A., Craig, W W., Christensen, F. E., et al. 2013, ApJ, 770, 103
Heinke, C. O., Rybicki, G. B., Narayan, R., & Grindlay, J. E. 2006, ApJ, 644, 1090
Hjellming, R. M. 1979, IAU Circ., 3369
Hjellming, R. M., Calovini, T. A., Han, X. H., et al. 1988, ApJ, 335, L75
Hua, X.-M., & Titarchuk, L. 1995, ApJ, 449, 188
Illarionov, A. F., & Sunyaev, R. A. 1975, A&A, 39, 185
Jansen, F., Lumb, D., Altieri, B., et al. 2001, A&A, 365, L1
Joss, P. C., & Li, F. K. 1980, ApJ, 238, 287
Kalberla, P. M., Burton, W. B., Hartmann, D., et al. 2005, A&A, 440, 775
Kaluzienski, L. J., Holt, S. S., & Swank, J. H. 1980, ApJ, 241, 779
Kennel, C. F., & Coroniti, F V. 1984, ApJ, 283, 710
King, A. R, Kolb, U., & Burderi, L. 1996, ApJ, 464, L127
Lasota, J.-P. 2001, New Astron. Rev., 45, 449
Lii, P. S., Romanova, M. M., Ustyugova, G. V., et al. 2013, MNRAS, submitted (arXiv:1304.2703)
Linares, M., Bahramian, A., Heinke, C., et al. 2014, MNRAS, 438, 251
Mahadevan, R., & Quataert, E. 1997, ApJ, 490, 605
Matsuoka, M., Inoue, H., Koyama, K., et al. 1980, ApJ, 240, L137
McClintock, J. E., & Remillard, R. A. 2000, ApJ, 531, 956
Menou, K., & McClintock, J. E. 2001, ApJ, 557, 304
Menou, K., Esin, A. A., Narayan, R., et al. 1999, ApJ, 520, 276
Narayan, R., & Yi, I. 1995, ApJ, 452, 710
Narayan, R., Mahadevan, R., & Quataert, E. 1998, in The Theory of Black Hole Accretion Disks, ed. M. A. Abramowicz, G. Bjornsson, & J. E. Pringle (Cambridge U. Press), 148 (arXiv:astro-ph/9803141)
Papitto, A., Ferrigno, C., Bozzo, E., et al. 2013, Nature, 501, 517
Patruno, A., Archibald, A. M., Hessels, J. W. T., et al. 2014, ApJ, 781, L3
Park, S., & Garcia, M. R. 2011, BAAS, 43, 144.25
Psaltis, D., & Chakrabarty, D. 1999, ApJ, 521, 332
Rutledge, R. E., Bildsten, L., Brown, E. F., Pavlov, G. G., & Zavlin, V. E. 1999, ApJ, 514, 945
Roberts, M. S. E. 2012, Proc. IAU Symp., 291, 127
Roberts, M. S. E., McLaughlin, M. A., Gentile, P., et al. 2014, preprint, arXiv:1402.5507
Roy, J., Bhattacharyya, B., & Ray, P. S. 2014, ATel, 5890
Rutledge, R. E., Bildsten, L., Brown, E. F., Pavlov, G. G., & Zavlin, V. E. 2002, ApJ, 577, 346
Rybicki, G. R., & Lightman, A. P. 1979, Radiative Processes in Astrophysics (New York, Wiley)
Schlafly, E. F., & Finkbeiner, D. P. 2011, ApJ, 737, 103
Shahbaz, T., Watson, C. A., & Dhillon, V. S. 2014, MNRAS, in press (arXiv:1402.1639)
Soria, R., Zampieri, L., Zane, S., & Wu, K. 2011, MNRAS, 410, 1886
Spruit, H. C. & Taam, R. E. 1993, ApJ, 402, 593
Stappers, B. W., Archibale, A. M., Hessels, J. W. T., et al. 2013, ApJ, submitted (arXiv:1311.7506)
Stappers, B. W., Gaensler, B. M., Kaspi, V. M., et al. 2003, Science, 299, 1372
Stella, L., Campana, S., Colpi, M., Mereghetti, S., & Tavani, M. 1994, ApJ, 423, L47
Strüder, L., Briel, U., Dennerl, K., et al. 2001, A&A, 365, L18
Tendulkar, S. P., Yang, C., An, H., et al. 2014, ApJ, submitted
Thorstensen, J. R., & Armstrong, E. 2005, AJ, 130, 759
Titarchuk, L. 1994, ApJ, 434, 313
Torres, M. A. P., Casares, J., Martinez-Pais, I. G., & Charles, P. A. 2002, MNRAS, 334, 233
Turner, M. J. L., Abbey, A., Arnaud, M., et al. 2001, A&A, 365, L27
Ustyugova, G. V., Koldoba, A. V., Romanova, M. M., et al. 2006, ApJ, 646, 304
van Paradijs, J. 1996, ApJ, 464, L139
Vaughan, S., Edelson, R., Warwick, R. S., & Uttley, P. 2003, MNRAS, 345, 1271
Verner, D. A., Ferland, G. J., Korista, K. T., & Yakovlev, D. G. 1996, ApJ, 465, 487
Wang, Z., Archibald, A. M., Thorstensen, J. R., et al. 2009, ApJ, 703, 2017
Wijnands, R., Degenaar, N., & Page, D. 2013, MNRAS, 432, 2366
Wik, D. R., Hornstrup, A., Molendi, S., et al. 2014, ApJ, submitted (arXiv:1403.2722)
Wilms, J., Allen, A., & McCray, R. 2000, ApJ, 542, 914
Zampieri, L., Turolla, R., Zane, S., & Treves, A. 1995, ApJ, 439, 849
Zampieri, L., Campana, S., Turolla, R., et al. 2001, A&A, 378, L5